

Disorder is good for you: the influence of local disorder on strain localization and ductility of strain softening materials

Dániel Tüzes · Péter Dusán Ispánovity · Michael Zaiser

Received: 21 July 2016 / Accepted: 23 January 2017 / Published online: 16 February 2017
© Springer Science+Business Media Dordrecht 2017

Abstract We formulate a generic concept model for the deformation of a locally disordered, macroscopically homogeneous material which undergoes irreversible strain softening during plastic deformation. We investigate the influence of the degree of microstructural heterogeneity and disorder on strain localization (formation of a macroscopic shear band) in such materials. It is shown that increased microstructural heterogeneity delays strain localization and leads to an increase of the plastic regime in the macroscopic stress–strain curves. The evolving strain localization patterns are characterized.

Keywords Fracture · Microstructures · Inhomogeneous material · Numerical algorithms · Probability and statistics

1 Introduction

Strain softening, loosely defined as a decrease of load carrying capability with increasing plastic deformation

of a material, leads to strain localization (formation of shear bands) which in turn may lead to catastrophic failure. If the width of the shear band is small as compared to the specimen dimensions, the macroscopic strain associated with the localized deformation may be small and failure occurs immediately after the material enters the softening regime. In materials where irreversible softening occurs shortly after yield, this may lead to a brittle appearance of the stress strain curves even though the failure mode is actually ductile. A most prominent example of this type of behavior are metallic glasses—a class of materials with potentially outstanding mechanical properties (Ashby and Greer 2006, for a recent overview of the mechanical behavior of metallic glasses, see also Schuh et al. 2007) but whose application is hindered by a propensity to fail shortly after yield by catastrophic shear band formation. The softening mechanism is in this case most likely associated with a shear-induced increase in free volume as originally proposed by Steif et al. (1982), though thermal softening associated with localized, adiabatic heating has been discussed as an alternative explanation, see e.g. Wright et al. (2001). A significant literature has been devoted to the question how the ductility of metallic glasses can be enhanced by delaying the onset of catastrophic shear localization. In this respect, numerous strategies have been explored that all rely on introducing some degree of nanoscale microstructural heterogeneity into the material. These include introducing a second interface phase (Adibi et al. 2013), embed-

D. Tüzes · P. D. Ispánovity
Department of Materials Physics, Eötvös University,
Pázmány Péter sétány 1/a, Budapest 1117, Hungary
e-mail: tuzes@metal.elte.hu

D. Tüzes · M. Zaiser (✉)
Institute for Materials Simulation (WW8),
Friedrich-Alexander-University, Erlangen-Nürnberg,
Dr.-Mack-Str. 77, 90762 Fürth, Germany
e-mail: michael.zaiser@fau.de

ding of nano-crystallites or isolated dendritic crystallites into a glassy matrix (Das et al. 2005; Hofmann et al. 2008; Xu et al. 2016), pre-straining along a different deformation path (Zhou et al. 2014; Wu et al. 2015), as well as micro-alloying to increase atomic-scale disorder by introducing quasi-point-defects (Qiao et al. 2016).

Metallic glasses are just one example of materials which exhibit local structural disorder—in this case down to the atomic scale. However, if one looks at defect microstructures, even crystalline solids exhibit (micro)structural disorder on scales well below the scale of a typical macroscopic specimen. On even larger scales, microstructural disorder is present in solid foams. In all these materials, one may legitimately ask how the macroscopic deformation behavior is influenced by the microstructural disorder and the associated length scales—which in the examples given may range from nanometers (for metallic glasses) up to millimetres for solid foams. For the case of transient softening, as observed in compression of metallic foams, it has been shown that increasing the microstructural heterogeneity may actually lead to a more homogeneous distribution of deformation on the macroscopic scale (Zaiser et al. 2013). In the present paper we consider a generic model which accounts for heterogeneity and randomness in the material microstructure and microstructure evolution, in conjunction with strain softening. The model builds upon the scalar plasticity model of Zaiser and co-workers (Zaiser and Moretti 2005; Zaiser and Aifantis 2006) which was originally introduced for single-slip deformation of crystals with disordered dislocation microstructure, but has recently been used by many authors to model the inception of shear bands in amorphous materials and the associated avalanche phenomena (see e.g. Talamali et al. 2012; Budrikis and Zapperi 2013; Sandfeld et al. 2015; Lin et al. 2015). We generalize this model to explicitly introduce a strain softening mechanism. We first describe the model and then use it to study how the simulated deformation behavior depends on the degree of microstructural disorder (scatter of the local flow stresses). In particular we study the strain localization process and the concomitant stress strain curves, which demonstrate that increasing the disorder can delay strain localization and thus lead to a significant increase in macroscopic ductility.

2 The stochastic continuum plasticity model

The model was originally formulated for single slip crystal plasticity. Accordingly, the plastic deformation state is characterized by a single scalar shear strain variable γ^{pl} . Without loss of generality we then assume the plastic strain tensor to be of the form $\epsilon^{\text{pl}}(\mathbf{r}) = \gamma^{\text{pl}}(\mathbf{r}) \mathbf{M}$ where $\gamma^{\text{pl}}(\mathbf{r})$ is the local plastic strain field and $\mathbf{M} = (\mathbf{e}_y \otimes \mathbf{e}_x + \mathbf{e}_x \otimes \mathbf{e}_y)/2$. The incremental dissipated work is given by $dW^{\text{diss}} = \tau d\gamma^{\text{pl}} = \sigma d\epsilon^{\text{pl}}$ where the shear stress $\tau(\mathbf{r}) := \sigma_{xy}(\mathbf{r})$.

In the present work we consider a 2D system where an infinitely extended specimen mimicked by periodic boundary conditions is, by remote boundary displacements, subject to a pure shear stress τ^{ext} in the xy plane. This 'external' stress superimposes on the 'internal' shear stress which derives from solving the Eigenstress problem associated with the inhomogeneous plastic strain field $\epsilon^{\text{pl}}(\mathbf{r})$. The local shear stress acting on a volume element at \mathbf{r} , which provides the driving force for plastic flow is then evaluated as $\tau^{\text{loc}}(\mathbf{r}) = \tau^{\text{int}}(\mathbf{r}) + \tau^{\text{ext}}$. For an infinite body, the solution of the Eigenstress problem can be evaluated as the convolution of the plastic strain with an elastic Green's function G^E , $\tau^{\text{int}}(\mathbf{r}) = (G^E * \gamma^{\text{pl}})(\mathbf{r})$ (Zaiser and Moretti 2005). For details of the actual evaluation procedure see Appendix.

The elastic domain is defined by the inequality

$$\Phi(\mathbf{r}) = \left| \tau^{\text{ext}}(\mathbf{r}) + (G^E * \gamma^{\text{pl}})(\mathbf{r}) \right| - \tau^c(\mathbf{r}) \leq 0. \quad (1)$$

The quantity Φ quantifies the difference between the shear stress acting at a given location \mathbf{r} and the local yield stress $\tau^c(\mathbf{r})$. As long as this quantity has a negative value, the material behaves locally in an elastic manner. Before specifying the evolution of plastic strain which occurs once the inequality (1) is violated, and the concomitant rules for assigning and evolving the local yield threshold $\tau^c(\mathbf{r})$, we first specify the implementation of the model on a two-dimensional discrete lattice.

2.1 Discretisation and stress evaluation

The Eq. (1) is space-discretised on a 2D lattice with square unit cell of area d^2 . The edges of the unit cell are oriented along the x and y directions. The total system is represented by a supercell of size $d^2(L \times L)$ which

is periodically continued in both x and y directions. To each cell (i, j) where the integers $i, j \in [1 \dots L]$ we assign a single value of the local shear strain, the local yield stress and the local stress. Where it is not noted otherwise, L is taken to be a power of two: $L = 2^n$.

The Green's function used for computing the internal shear stress is denoted by $G^E(\mathbf{r})$ for the space-continuous case and by $G_{i,j}^E = G(i\mathbf{e}_x + j\mathbf{e}_y)$ for the space-discrete case; the indices $(0, 0)$ correspond to $\mathbf{r} = 0$. Because of stress equilibrium, the conditions $\int G^E(\mathbf{r})d^2r = 0$ must be fulfilled for the space-continuous and $\sum_{ij} G_{i,j}^E = 0$ for the space-discrete case. The internal stress acting in cell (i, j) is evaluated as

$$\tau_{i,j}^{\text{int}}(t) = \sum_{k,l=1}^L G_{k-i,l-j}^E \gamma_{k,l}^{\text{pl}}(t). \quad (2)$$

Here $\gamma_{k,l}^{\text{pl}}$ is the plastic shear strain in the cell (k, l) . The calculation of the periodically continued stress kernel $G_{i,j}^E$ is detailed in the Appendix.

The external stress is controlled by remote displacements acting on the system which impose a total (elastic and plastic) shear strain γ^{tot} . Since the average of all internal stresses is by construction zero, stress equilibrium requires that

$$\tau^{\text{ext}} = \mu (\gamma^{\text{tot}} - \gamma^{\text{pl}}), \quad \gamma^{\text{pl}} = \frac{1}{L^2} \sum_{k,l=1}^L \gamma_{k,l}^{\text{pl}}, \quad (3)$$

where μ is the shear modulus.

2.2 Stochastic flow rule

Plastic deformation is assumed to proceed in discrete, localized events which occur whenever the inequality, Eq. (1) is locally violated. If this is the case for any site (k, l) , we increase the plastic strain $\gamma_{k,l}^{\text{pl}}$ at this site instantaneously by

$$\Delta\gamma_{k,l}^{\text{pl}} = \min(\Delta\gamma_0, \Delta\gamma_{k,l}^*), \quad \Delta\gamma_{k,l}^* = \Delta\gamma_0 \frac{\tau_{k,l}^{\text{int}} + \tau^{\text{ext}}}{|G_{0,0}^E|}. \quad (4)$$

where $G_{0,0}^E = -2\mu/[\pi(1-\nu)]$ (see Appendix). This means that the strain is increased by a value that sets

the local stress to zero if this value is less than $\Delta\gamma_0$, or otherwise by $\Delta\gamma_0$. In this manner we ensure that the increment dW^{diss} of the locally dissipated work is always positive as required by the second law of thermodynamics.

Local structural disorder is taken into account in terms of random variations of the local flow threshold τ^c . We assume that the system is statistically homogeneous and that the size of a cell is larger than the spatial correlation range of the microstructural disorder that gives rise to local yield stress variations. Hence, the local yield stresses are considered as independent, identically distributed random variables $\tau_{k,l}^c$ which we take to be Weibull distributed with exponent β and mean value τ_0^c ; larger β implies a smaller scatter of local yield stresses, i.e., a lower degree of microstructural disorder in the material. Independent values of $\tau_{k,l}^c$ are initially assigned to all sites. Plasticity-induced changes in the local flow threshold are taken into account by assigning, after each local strain increment occurring at a site of the simulation grid, to this site a new local yield stress. Specifically, we draw a new value from the same distribution with average τ_0^c and multiply this with a strain dependent factor $F(\gamma_{k,l}^{\text{pl}}) = 1 - f\gamma_{k,l}^{\text{pl}}$ where $f < 0$ is a softening parameter (conversely, linear hardening could be implemented by assuming negative f).

2.3 Simulation protocol

We non-dimensionalize the model by measuring all stresses in units of the mean flow threshold τ_0^c , all strains in units of τ_0^c/μ (elastic strain needed to reach the mean flow threshold, divided by the shear modulus), and spatial coordinates in units of the cell size d . The model behaviour is then, in addition to the Weibull parameter β , controlled by a single numerical parameter $I = |G_{0,0}^E|\Delta\gamma_0/\tau_0^c$ (henceforth: 'coupling constant') which controls the magnitude of the internal-stress re-distribution after a deformation event relative to the average flow stress. In the following we make the simplifying assumption that $\nu = 0.353$ in which case $I = \mu\Delta\gamma_0/\tau_0^c$ equals the scaled local strain increment. The local stress reduction at the site of a unit deformation event is then I and the external stress reduction associated with the same event is I/L^2 .

Simulations are performed as follows: we assign initial flow thresholds to all sites according to the prescribed Weibull distribution with exponent β and mean

value 1. We then determine the site with the lowest threshold and increase the total strain γ^{tot} such that the concomitant stress increase as given by Eq. (3) exactly matches the threshold, triggering the first deformation event. After the event, which is supposed to occur instantaneously, we re-compute all stresses while keeping γ^{tot} fixed, evaluate the local values of the yield threshold $\Phi_{k,l}$ for all sites, and check whether there are additional sites which become unstable ($\Phi_{k,l} > 0$). If yes we increase, still at fixed γ^{tot} , the strain at the unstable site with the largest value of $\Phi_{k,l}$, thus implementing an extremal dynamics. We repeat this until there are no more unstable sites (the avalanche has terminated). The plastic strain and the stress at this point are evaluated from Eq. (3). We then determine again the site with the smallest threshold, and increase γ^{tot} such that the concomitant stress increase as given by Eq. (3) makes this site unstable and triggers the next avalanche. We repeat this cycle of avalanche triggerings until the local strain of at least one site reaches the value $\gamma_{k,l}^{\text{pl}} = 1/f$ such that the strength of this site becomes zero. This is tantamount to the nucleation of a microcrack which we take as a signature of impending system failure. The concomitant average plastic strain defines the system failure strain γ_f^{pl} .

3 Results

Simulations were performed for Weibull shape parameters $\beta = 1, 2, 4$, and 8 , coupling constants $I = 0.125, 0.25, 0.5$, and 1 , and for system sizes $L = 32, 64, 128, 256$, and 512 . In each case ensembles of 512 simulations with statistically independent initial conditions were performed. The softening parameter f was kept fixed at $f = 1/16$.

3.1 Stress–strain curves

Average stress–strain curves were obtained by averaging the external stress at a given deformation over the simulations as shown in Fig. 1.

The curves exhibit three different regimes: an initial quasi-elastic loading regime is followed by a transition to a plastic deformation regime where the stress increases with strain (hardening regime). The elastic and hardening regimes are system size independent. The hardening regime is followed by a transition to a

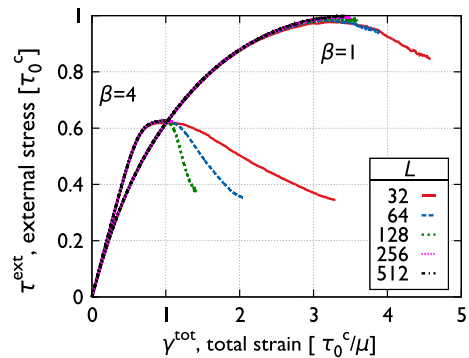


Fig. 1 Stress–total strain curves for two different yield-stress distributions (Weibull exponents $\beta = 1$ and $\beta = 4$) and different system sizes; other parameters $I = 1$; $f = 1/16$

softening part where the stress decreases with macroscopic strain. The simulations are terminated once microcrack nucleation occurs as indicated by a complete loss of strength at one or more sites. The corresponding failure strains are much below the expectation $\gamma_f^{\text{pl}} = 16$ for a homogeneous system, indicating a significant degree of deformation localization. We also observe that the softening regime is system size dependent: The stress decrease occurs more rapidly and failure occurs at lower strains in larger systems. Such system size dependence again indicates some kind of deformation localization. We therefore proceed to investigate the strain patterns that emerge in the different deformation stages.

3.2 Patterns in the strain maps

Figure 2 illustrates the changes in the strain patterns that occur during the softening regime. At the peak stress before the onset of softening, deformation is macroscopically homogeneous but exhibits mesoscale patterns in the form of numerous diffuse shear bands which follow the planes of maximum shear stress, here aligned with the x and y directions. These patterns are more pronounced with increasing degree of disorder. Note that the peak stress is reached later in the more disordered sample (top left graph in Fig. 2), hence the overall strain is bigger. During the softening regime we observe a qualitative change in the patterns as most of the additional strain accruing during the softening regime is localized in a single shear band which also contains the location where microcrack nucleation takes place.

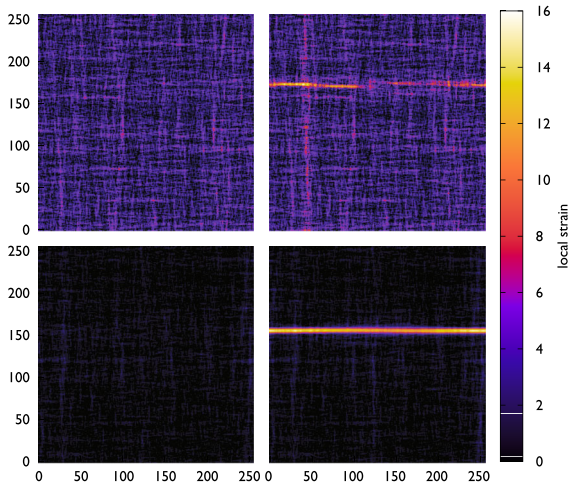


Fig. 2 Strain patterns at the highest external stress just before the onset of softening (left) and at the end of the simulation (right); $\beta = 1$ (top) and $\beta = 4$ (bottom); other parameters: $I = 1, f = 1/16, L = 256$

This shear band is sharper and more pronounced in the sample with less disorder (bottom right graph in Fig. 2).

The formation of a localized shear band is in line with the ideas of classical continuum mechanics which predicts localization to occur, in a system without boundary constraints and under pure shear loading, at the transition from strain hardening to strain softening regimes. To better characterize this behavior we now seek to define a quantitative measure for the strain localization process.

3.3 Deformation localisation

In order to quantify strain localisation we investigate the spatial distribution of the incremental strain. We divide the average stress–strain curve into $n = 50$ intervals, the k th interval is defined by $\gamma^{pl} \in [\gamma^{pl,k}, \gamma^{pl,k+1})$, $\gamma^{pl,k} = k \langle \gamma_f^{pl} \rangle / n$. The plastic strain increase occurring at the site (i, j) during strain interval k is denoted as $\gamma_{i,j}^{pl,k}$.

We now use that a shear band has a planar shape. For any given plane \mathcal{P} we can define a scalar measure of distance which characterizes the distribution of the incremental strain with respect to the plane. To this end we denote the distance between site (i, j) and the plane \mathcal{P} as $d_{i,j}^{\mathcal{P}}$. (Because of the periodic boundary conditions used, we evaluate $d_{i,j}^{\mathcal{P}}$ as the minimum distance

between the site (i, j) and any of the periodic images of \mathcal{P}). We now define the strain-weighted average of $d_{i,j}^{\mathcal{P}}$ as

$$[d_k^{\mathcal{P}}]_{\gamma} = \frac{\sum_{ij} \gamma_{i,j}^{pl,k} \cdot d_{i,j}^{\mathcal{P}}}{\sum_{ij} \gamma_{i,j}^{pl,k}}. \tag{5}$$

For a completely homogeneous distribution of the plastic strain increment, we have $[d_k^{\mathcal{P}}]_{\gamma} = L/4$ for all planes \mathcal{P} . For a heterogeneous distribution we identify the plane for which $[d_k^{\mathcal{P}}]_{\gamma}$ has the smallest value and define a localization parameter η as

$$\eta_k = 1 - \frac{4}{L} \min_{\mathcal{P}} [d_k^{\mathcal{P}}]_{\gamma}. \tag{6}$$

This parameter takes the value $\eta_k = 0$ for a statistically homogeneous distribution of the plastic strain increment, and the value $\eta_k = 1$ if the incremental strain is completely localized on a single plane.

It can be seen in Fig. 3 that in all simulations the localization parameter η starts at $\eta = 0$ and then gradually increases during the hardening regime. Immediately after the peak stress is reached and the system enters the macroscopic softening regime, η increases rapidly towards $\eta = 1$, indicating the localization of deformation in a single shear band. The comparison of the strain evolution of η and τ^{ext} clearly demonstrates the correlation. It is equally evident that an increasing degree of disorder (decrease of the Weibull exponent from $\beta = 8$ to $\beta = 1$), even though it leads to an earlier onset of plastic flow, extends the hardening regime to larger strains and delays the onset of deformation localization. The role of the coupling constant I , which reflects the magnitude of the local strain increment, is more ambiguous: for small disorder, large values of I promote localization whereas for large disorder, the opposite is the case.

We now look at the distribution of incremental strain around the final failure plane. This is shown in Fig. 4 which depicts shear band profiles for large disorder ($\beta = 1$) and for small disorder ($\beta = 8$), recorded for different values of the localization parameter η . The width of the shear band is almost the same in both cases, however, localization of deformation around the final failure plane happens later in case of large disorder. This looks strange at first glance, given that the curves compare situations with equal value of η , however, the

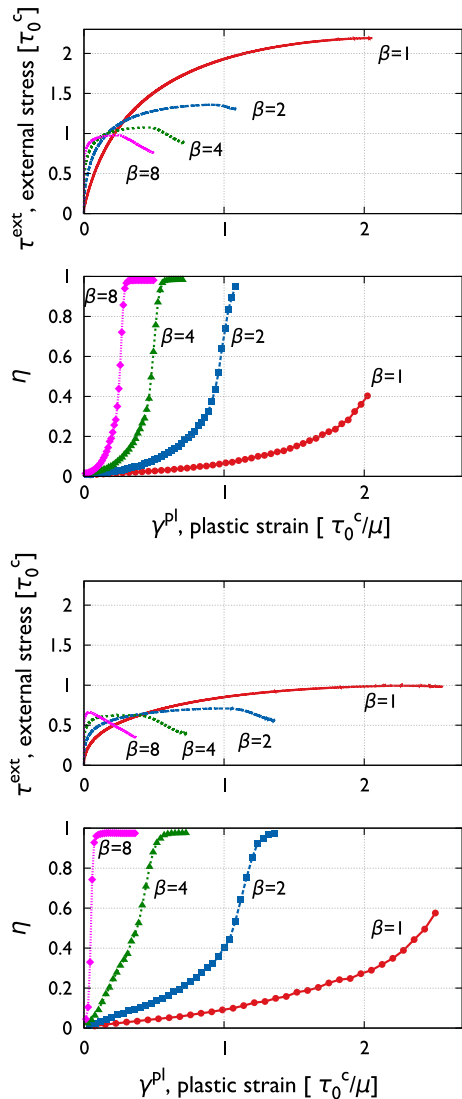


Fig. 3 Stress strain curves and strain evolution of the localization parameter η for different degrees of disorder (Weibull parameter $\beta \in [8, 4, 2, 1]$). The upper two figures correspond to $I = 0.125$, the lower two ones to $I = 1$

reason is simple: In case of large disorder, deformation first localizes in a transient manner (i.e., on slip planes that are in general *not* close to the final failure plane) and localization on the final failure plane happens after extensive deformation activity has occurred elsewhere. In case of small disorder, by contrast, deformation localizes on the final failure plane almost from the onset.

We note that the localization measure used here, which measures localization with respect to a best-fit

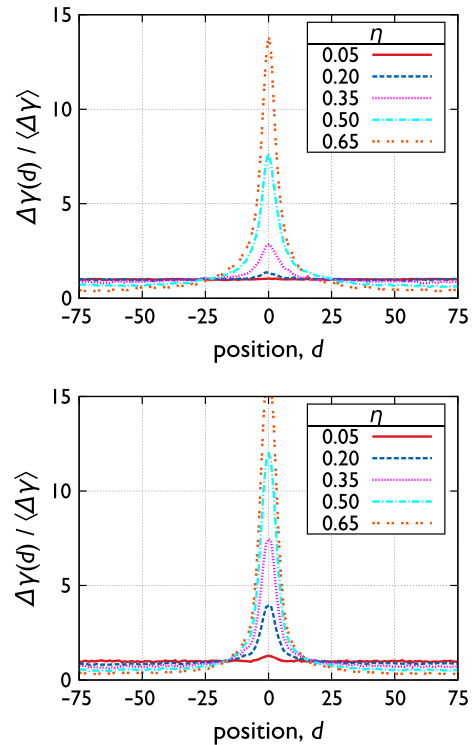


Fig. 4 Evolution of the distribution of strain around the final failure plane for Weibull parameters $\beta = 1$ (upper) and $\beta = 8$ (lower). Other parameters: $I = 1$, $f = 1/16$, $L = 256$

shear plane, is analogous to the one used by [Lennartz-Sassinek et al. \(2014\)](#) for the analysis of strain localization and failure processes in rock samples. This criterion is quite different from other measures proposed in the literature, in the sense that it accounts for the spatial distribution of the heterogeneous deformation. If we compare with the naive measure provided by the root-mean-square deviation of the local from the average plastic strain (see e.g. [Cheng et al. 2009](#)), it is evident that the latter measure—which accounts for the magnitude of the scatter but not for its spatial distribution—cannot distinguish between a single broad shear band and numerous, spatially distributed narrow ones which carry the same local strain. This distinction is, however, central to our argument (‘disorder is good for you’) which states that a large degree of small-scale microstructural heterogeneity *increases* heterogeneity at the smallest scales but prevents, on the largest scale, the emergence of heterogeneity in the form of a single macroscopic shear band which leads to sample failure.

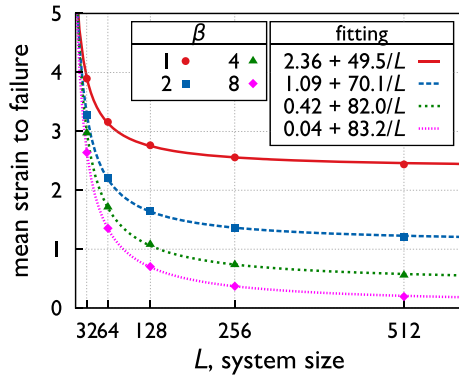


Fig. 5 Mean strain at failure as a function of system size, for different Weibull parameters; *dashed lines* fit curves $\gamma_f = c_1 + c_2/L$

3.4 Mean strain to failure

The beneficial effect of disorder on ductility is also borne out when we consider the mean strain at failure. This strain is system size dependent and decreases with increasing system size. This dependency can be rationalized by making the simplifying assumption that the system deforms homogeneously during the hardening regime, accumulating a homogeneous strain γ_h , whereas all strain accruing during the subsequent softening regime is localized in a slip band of finite width d_β . Failure occurs once the plastic strain in the band reaches the value γ_f^{loc} . Then the mean strain at failure is $\gamma_f = \gamma_h + (\gamma_f^{loc} - \gamma_h)(d/L)$. We can thus fit the system size dependence as $\gamma_f = c_1 + c_2/L$ where the parameter c_1 defines the homogeneous strain γ_h which is also the failure strain in the infinite system limit. This strain is plotted in Fig. 6 as a function of the Weibull exponent β . Again we see that larger microstructural disorder leads to an increase in ductility of the strain softening material. For large systems ($L \rightarrow \infty$) the increase is quite dramatic—between Weibull exponent $\beta = 8$, corresponding to a coefficient of variation of 0.148, and Weibull exponent $\beta = 1$ (coefficient of variation 1), the strain to failure increases in this limit by a factor of about 60.

3.5 A local criterion for shear band growth

Failure of a macroscopic system occurs once the first macroscopic (system spanning) shear band forms and deformation localizes there. However, embryonic shear

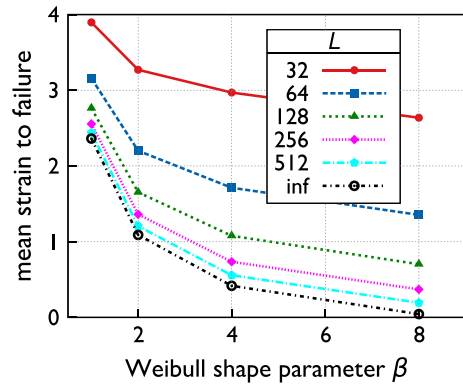


Fig. 6 Mean strain at failure as a function of the Weibull shape parameter β , for different system sizes. The value for infinitely large system size is obtained from the parameter c_1 of the fit curves in Fig. 5

bands are present already before the onset of softening (Fig. 2). At this point we ask whether we can establish a criterion which allows us to better understand the conditions for the emergence of a macroscopic shear band. To this end we assume a pre-existing shear band of some extension and investigate its growth. The stress concentration at the tip of a straight band with a width of one cell can be estimated as

$$\tau_{tip} = \sum_{k=1}^{\infty} G_{k,0}^E \approx 0.385 G_{0,0}^E \tag{7}$$

The band expands if this stress concentration triggers a deformation event at one of the sites ahead of either tip. The stress needed to activate a site is given by $\Delta\tau = -\Phi$ (we might also call this the residual strength of the site), and the probability that a randomly chosen site is activated by a stress increment τ^* is $P(\Delta\tau < \tau^*)$. We now investigate the evolution of the probability $P(\Delta\tau < \tau_{tip})$ (i.e, the probability that an advance of a band triggers another advance straight ahead) as a function of strain. Figure 7 indicates that this probability increases continually with increasing strain until it reaches a level of about $P(\Delta\tau < \tau_{tip}) \approx 0.3$ which does not depend on the model parameters (disorder parameter β , coupling constant I). At this critical value, $P(\Delta\tau < \tau_{tip})$ suddenly drops. This drop coincides with the formation of a system spanning shear band where deformation localizes: the associated stress drop reduces the value of $P(\Delta\tau < \tau_{tip})$ everywhere except in the band itself where the local strain soften-

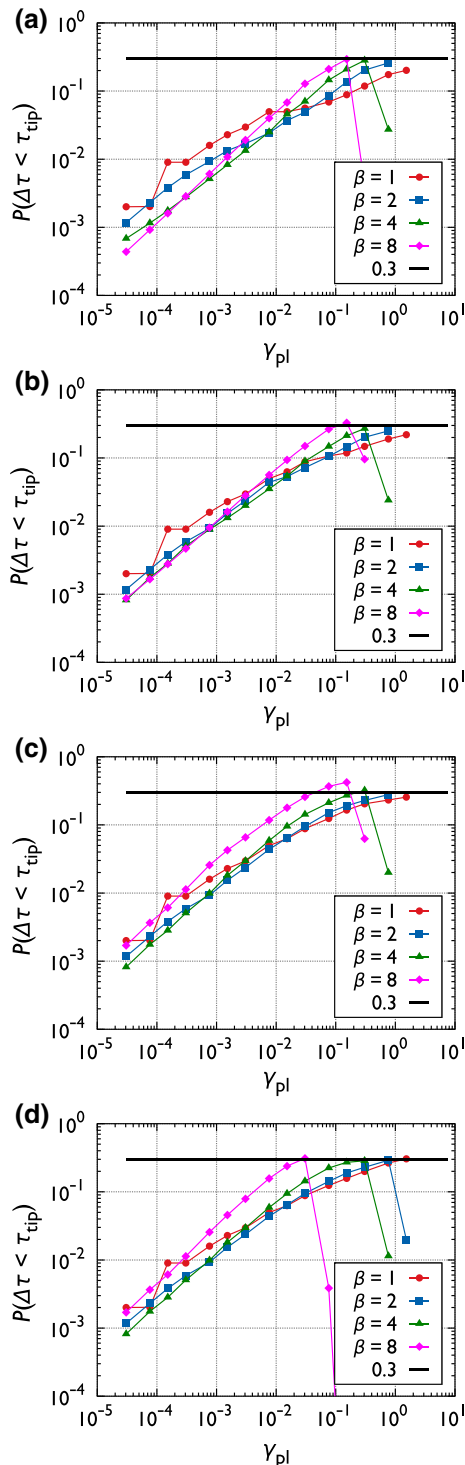


Fig. 7 Evolution of the triggering probability $P(\Delta\tau < \tau_{\text{tip}})$ at the tip of an incipient shear band. **a** $I = 0.125$, **b** $I = 0.25$, **c** $I = 0.5$ and **d** $I = 1$

ing maintains it at the critical level for sustained shear band operation.

Despite significant variations in the distributions $P(\Delta\tau < \tau^*)$ which depend strongly on the disorder parameter β , we observe that the critical value of $P(\Delta\tau < \tau_{\text{tip}})$ is quite universal. This leads us to the conclusion that shear band growth is driven by processes occurring at the tip of an incipient shear band, and that it depends on the interaction of the shear band tip with the local distribution of the residual strength whether or not shear band growth can occur. Indeed, if we account for the fact that shear bands may grow at both tips, and that growth may not necessarily be constrained to expansion straight ahead but may occur via sideways deflection (thus, at each tip there may be three sites available for continuing growth), we can estimate that a critical probability of the order of $1/3$ for triggering a site at the crack tip may be sufficient for sustained growth of a shear band.

Thus our analysis leads us to envisaging shear band formation as essentially a two-stage process: In a first stage, local yielding and the concomitant stress re-distribution lead to a system-wide re-shuffling of the residual strength distribution in such a manner that the triggering probability $P(\Delta\tau < \tau_{\text{tip}})$ at the tip of an incipient shear band gradually increases. During this stage, deformation is macroscopically homogeneous, even though shear band nuclei are continuously forming and getting again inactivated. The duration of this latency stage depends on the degree of disorder and increases with increasing disorder parameter β . As soon as the triggering probability reaches a critical value $P(\Delta\tau < \tau_{\text{tip}}) \approx 0.3$, a transition to a second stage occurs where the flow process is governed by the rapid formation of a system-spanning shear band where deformation localizes. In large systems, this leads to near-instantaneous failure.

It may be noted in passing that the residual strength probability distribution $P(\Delta\tau < \tau^*)$, notably its behavior near the edge of stability, $\Delta\tau \rightarrow 0$, has recently been conjectured by Lin et al. (2014, 2015) to play a crucial role in the dynamics of similar models as the present one but *without* softening. In these works it is argued that the spatial organization of slip in shear bands is largely irrelevant during the approach to failure, and that the non-local elastic kernel can be approximated by a random stress re-distribution in a mean-field model which by construction destroys any spatial correlations. Our observations, by contrast, point to the

importance of correlated shear band growth in controlling system stability as soon as some degree of softening is introduced into the model.

4 Discussion and conclusions

We studied the deformation and failure behavior of microstructurally disordered model materials which exhibit irreversible strain softening and therefore fail by shear band formation. Contrary to the intuitive idea that increased microstructural heterogeneity may facilitate shear band nucleation and therefore have a negative impact on deformability, we find a strong positive effect of increased heterogeneity and randomness on the deformation properties. Increased microstructural heterogeneity indeed leads to an earlier onset of deformation in the form of diffuse shear bands—an effect that is easily understood within the classical paradigm of weakest-link statistics (for a discussion in the plasticity context see e.g. [Ispánovity et al. 2013](#)). However, the same heterogeneity prevents the spreading of shear bands and their coalescence into a system spanning macro-shear-band. The earlier onset of deformation is matched by an extended hardening regime, associated with the elimination of weak regions from the microstructure. This hardening can be envisaged as a survival-bias-hardening (easily deformable configurations are eliminated, stronger configurations survive) and becomes more pronounced with increasing scatter in local strength. Only after the survival-bias-hardening is exhausted, structural softening takes over and promotes macroscopic deformation localization. In line with classical concepts of continuum mechanics of homogeneous materials, the onset of macroscopic localization neatly coincides with the peak stress where the system enters the softening regime of the stress strain curve.

Our findings indicate that, in microstructurally disordered materials where ductility is limited by shear band formation, it may be a good idea to *increase* the degree of microstructural heterogeneity on the nanoscale as such an increase results both in an increase in strength and in a very significant increase in ductility. In the context of metallic glasses, our findings match well with ideas to increase the ductility of metallic glasses by introducing a second interface phase ([Adibi et al. 2013](#)) or by embedding nano-crystallites or isolated dendritic crystallites into a glassy matrix ([Das](#)

[et al. 2005](#); [Hofmann et al. 2008](#))—ideas which are tantamount to increasing the scatter of local deformation properties within a generally disordered microstructure. From a computational point of view such ideas have been until now mainly been studied by means of molecular dynamics simulations which indeed indicate that introduction of nanoscale heterogeneities such as glass-glass interfaces can promote the nucleation of multiple shear bands and thus mitigate against catastrophic shear localization in a single band, see in particular the work of [Şopu et al. \(2011\)](#), [Albe et al. \(2013\)](#). Unfortunately such simulations can, owing to the limited spatial and temporal scales that can be reached in MD simulations, not easily be carried to the level of a direct investigation of macroscopic strain localization phenomena. At the same time, MD simulations can be used to parameterize mesoscopic models such as the present one, as shown notably by [Rodney \(2009, 2011\)](#); [Albaret et al. \(2016\)](#). An important line of development of the present work may consist in combining the present mesoscale model with MD simulations to obtain physically based parameters for the model for bulk metallic glasses as well as for nanoglasses and amorphous nanocomposite structures.

Of course, it is a well established idea that strong-yet-ductile materials can be engineered by combining weak-but-ductile and strong-but-brittle components into heterogeneous composite microstructures. However, this is not what we are studying in the present work: as manifest from the constitutive relation of our model material, volume elements of different strength are assumed to fail at the same local strain. If we investigate the evolution of the final, macroscopic shear band, then we can see little difference between weakly disordered and strongly disordered microstructures (Fig. 4). Nevertheless, the overall deformation behavior is radically different in both cases, because enhanced disorder leads to an extended regime of diffuse shear band formation and delays the coalescence of local shear band nuclei into a macroscopic shear band. To understand this behavior it is in our opinion necessary to move towards an understanding of the manner how fluctuations emerge and extend across scales. This viewpoint is corroborated by investigations of models similar to the present one which demonstrate the emergence of scale-free, system spanning correlations in the internal stress and local strain patterns ([Zaiser 2006](#); [Kapetanou et al. 2015](#)). As a consequence of such correlations, the emergent macroscopic materials behavior can neither

be inferred from local statistics (e.g. using weakest-link arguments) nor can it be easily related to the properties of a small, circumscribed representative volume element. Thus, novel conceptual tools may be needed to exploit the possibilities created for improving materials performance by exploiting the manner in which local fluctuations in materials properties may not only influence, but qualitatively change the macroscopic behavior of materials.

Acknowledgements Financial support of the Hungarian Scientific Research Fund (OTKA) under contract number PD-105256 and of the European Commission under Grant Agreement No. CIG-321842 are also acknowledged. DT is supported by a One Year scholarship program sponsored by the Free State of Bavaria for graduates of Central, Eastern and Southeastern European states. PDI is also supported by the János Bolyai Scholarship of the Hungarian Academy of Sciences. MZ acknowledges financial support of DFG under Grant No. Za171/8-1.

Appendix

In our evaluation of internal stresses we use that the evaluation of stresses in any plane strain deformation problem can be mapped onto the evaluation of the stress field of a 2D dislocation arrangement consisting of straight parallel edge dislocations with line direction perpendicular to the considered plane. In particular, the shear stress field $\sigma_{xy}(\mathbf{r}) =: \tau(\mathbf{r})$ generated by a two dimensional distribution of dislocations with Burgers vector parallel to the x axis, line direction along the z axis, and Burgers vector density α can be expressed as

$$\tau(\mathbf{r}) = \int \tau_{\text{ind}}(\mathbf{r} - \mathbf{r}') \alpha(\mathbf{r}') d^2r' \tag{8}$$

where τ_{ind} is the shear stress field created by a dislocation of unit Burgers vector length,

$$\tau_{\text{ind}}(\mathbf{r}) = \frac{\mu}{2\pi(1-\nu)} \frac{x(x^2 - y^2)}{(x^2 + y^2)^2}. \tag{9}$$

Due to the relation $\alpha = -\partial_x \gamma(\mathbf{r})$ (Groma et al. 2003), the shear stress field can then be expressed in terms of the shear strain field as

$$\tau(\mathbf{r}) = - \int \tau_{\text{ind}}(\mathbf{r} - \mathbf{r}') \partial_x \gamma(\mathbf{r}') d^2r'. \tag{10}$$

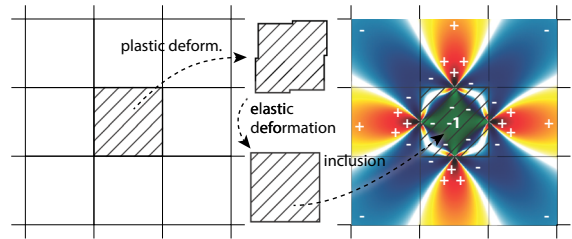


Fig. 8 In the elementary slip event, a cell is cut into four pieces which are displaced according to the acting shear stress and then glued back together. This cell is inserted back into the original lattice and forced elastically to fit, generating an internal stress field

By a partial integration one obtains

$$\tau(\mathbf{r}) = \int \gamma(\mathbf{r}') \partial_x \tau_{\text{ind}}(\mathbf{r} - \mathbf{r}') d^2r'. \tag{11}$$

Here $\partial_x \tau_{\text{ind}}(\mathbf{r}) = G^E$ is the Green's function which allows to calculate the shear stress by convolution with the strain.

We now need to adapt the above reasoning to a discrete lattice system with periodic boundary conditions. In doing so we aim at a correct representation on large scales, and at a correct representation of the symmetries of the Green's function, but not at a faithful representation of the shearing process *inside* a single grid cell (which cannot be represented anyway in a lattice based simulation). Thus we calculate the stress and strain fields generated by an elementary slip event in a cell as follows (Fig. 8 illustrates the calculation.) The cell under deformation is cut along the x and y direction. The upper part is moved by a distance b along the x direction and the right side is moved by b along the y direction, according to the sign of the shear stress acting on the cell. Then, the four parts are glued back together. Next, an elastic deformation is applied which transforms the cell back to its original shape so it fits its original place in the sample. The cell is placed back to its original position and the sample is elastically relaxed. The average plastic strain generated by this process in the cell is $\Delta\gamma^{\text{pl}} = 2b/d$.

The process is formally equivalent to adding four edge dislocations with the respective virtual Burgers vectors $be_x, be_y, -be_x, -be_y$ at the centerpoints of the right, top, left and bottom sides of the cell. Accordingly, the stress field can be evaluated as the superposition of the stress fields of these four dislocations. Peri-

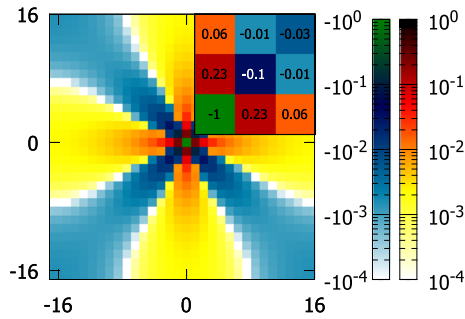


Fig. 9 The stress field of a unit slip event located in the origin in the units of $|G_{0,0}^E|$, assuming periodic boundary conditions with $L = 32$. Note the symmetry in the x and y directions and the logarithmic color scale. In the upper right corner we show a magnification for $k \in [0, 2]$, $l \in [0, 2]$

odic boundary conditions are implemented by adding to the stress fields of the four dislocations those of their periodic images which form an infinite lattice of period L (for details of the method used for evaluating the lattice sum, see Bako et al. 2006). We evaluate stresses at the cell centerpoints, hence, the stress field induced by a elementary slip event $\Delta\gamma^{\text{pl}}$ at the centerpoint of the active cell is obtained from summation of the stress fields of the four edge dislocations as $G_{0,0}^E \Delta\gamma^{\text{pl}} = -2\mu \Delta\gamma^{\text{pl}} / [\pi(1-\nu)]$ where μ is the shear modulus and ν is Poisson's ratio. The result is shown in Fig. 9.

We emphasize that the use of dislocations to evaluate internal stresses is, in our present context, a mere computational device which allows us to treat the periodic boundary conditions in a simple and efficient manner, but which does not necessarily reflect the physical processes which govern the elementary slip event $\Delta\gamma^{\text{pl}}$ (e.g., in the context of amorphous materials, this could be a shear transformation which does not involve any dislocations).

References

- Adibi S, Sha Z, Branicio P, Joshi SP, Liu Z, Zhang Y (2013) A transition from localized shear banding to homogeneous superplastic flow in nanoglass. *Appl Phys Lett* 103(211):905
- Albaret T, Tanguy A, Bolioli F, Rodney D (2016) Mapping between atomistic simulations and Eshelby inclusions in the shear deformation of an amorphous silicon model. *Phys Rev E* 93(053):002. doi:10.1103/PhysRevE.93.053002
- Albe K, Ritter Y, Soppa D (2013) Shear band formation, nanocomposites and nanoglasses investigated by molecular dynamics simulations. *Mech Mater* 67:94–103
- Ashby M, Greer A (2006) Metallic glasses as structural materials. *Scripta Mater* 54(3):321–326. doi:10.1016/j.scriptamat.2005.09.051
- Bako B, Groma I, Györgyi G, Zimanyi G (2006) Dislocation patterning: the role of climb in meso-scale simulations. *Comput Mater Sci* 38:22–28
- Budrikis Z, Zapperi S (2013) Avalanche localization and crossover scaling in amorphous plasticity. *Phys Rev E* 88(062):403. doi:10.1103/PhysRevE.88.062403
- Cheng Y, Cao A, Ma E (2009) Correlation between the elastic modulus and the intrinsic plastic behavior of metallic glasses: the roles of atomic configuration and alloy composition. *Acta Mater* 57(11):3253–3267. doi:10.1016/j.actamat.2009.03.027
- Das J, Tang M, Kim KB, Theissmann R, Baier F, Wang WH, Eckert J (2005) “Work-hardenable” ductile bulk metallic glass. *Phys Rev Lett* 94(205):501
- Groma I, Csikor F, Zaiser M (2003) Spatial correlations and higher-order gradient terms in a continuum description of dislocation dynamics. *Acta Mater* 51(5):1271–1281. doi:10.1016/S1359-6454(02)00517-7
- Hofmann DC, Suh JY, Wiest A, Duan G, Lind ML, Demetriou MD, Johnson W (2008) Designing metallic glass matrix composites with high toughness and tensile ductility. *Nature* 451:1085–1089
- Ispánovity PD, Ádám Hegyi, Groma I, Györgyi G, Ratter K, Weygand D (2013) Average yielding and weakest link statistics in micron-scale plasticity. *Acta Mater* 61(16):6234–6245. doi:10.1016/j.actamat.2013.07.007
- Kapetanou O, Weygand D, Zaiser M (2015) Stress and strain fluctuations in plastic deformation of crystals with disordered microstructure. *J Stat Mech Theory Exp* P08009
- Lennartz-Sassinek S, Main IG, Zaiser M, Graham CC (2014) Acceleration and localization of subcritical crack growth in a natural composite material. *Phys Rev E* 90(052):401. doi:10.1103/PhysRevE.90.052401
- Lin J, Saade A, Lerner E, Rosso A, Wyart M (2014) On the density of shear transformations in amorphous solids. *EPL (Europhys Lett)* 105(2):26003
- Lin J, Gueudre T, Rosso A, Wyart M (2015) Criticality in the approach to failure in amorphous solids. *Phys Rev Lett* 115:168,001. doi:10.1103/PhysRevLett.115.168001
- Qiao J, Yao Y, Pelletier J, Keer L (2016) Understanding of microalloying on plasticity in $\text{Cu}_{46}\text{Zr}_{47-x}\text{Al}_7\text{dy}$, $0 \leq x \leq 8$ bulk metallic glasses under compression: based on mechanical relaxations and theoretical analysis. *Int J Plast* doi:10.1016/j.ijplas.2016.02.002S0749641916300122
- Rodney D, Schuh C (2009) Distribution of thermally activated plastic events in a flowing glass. *Phys Rev Lett* 102(235):503
- Rodney D, Tanguy A (2011) Modeling the mechanics of amorphous solids at different length scale and time scale. *Modell Simul Mater Sci Eng* 19(083):001
- Sandfeld S, Budrikis Z, Zapperi S, Fernandez Castellanos D (2015) Avalanches, loading and finite size effects in 2D amorphous plasticity: results from a finite element model. *J Stat Mech Theory Exp* 2015(2):P02011

- Schuh CA, Hufnagel TC, Ramamurty U (2007) Mechanical behavior of amorphous alloys. *Acta Mater* 55:4067–4109
- Şopu D, Ritter Y, Gleiter H, Albe K (2011) Deformation behavior of bulk and nanostructured metallic glasses studied via molecular dynamics simulations. *Phys Rev B* 83(100):202. doi:[10.1103/PhysRevB.83.100202](https://doi.org/10.1103/PhysRevB.83.100202)
- Steif P, Spaepen F, Hutchinson JW (1982) Strain localization in amorphous metals. *Acta Metall* 30(2):447–455
- Talamali M, Petäjä V, Vandembroucq D, Roux S (2012) Strain localization and anisotropic correlations in a mesoscopic model of amorphous plasticity. *C R Mécanique* 340(4–5):275–288. doi:[10.1016/j.crme.2012.02.010](https://doi.org/10.1016/j.crme.2012.02.010) (recent *Adv Micromech Mater*)
- Wright W, Schwarz RB, Nix W (2001) Localized heating during serrated plastic flow in bulk metallic glasses. *Mater Sci Eng A* 319:229–232
- Wu Y, Bei H, Wang Y, Lu Z, George E, Gao Y (2015) Deformation-induced spatiotemporal fluctuation, evolution and localization of strain fields in a bulk metallic glass. *Int J Plast* 71:136–145. doi:[10.1016/j.ijplas.2015.05.006](https://doi.org/10.1016/j.ijplas.2015.05.006)
- Xu X, Wang Y, Guo A, Geng H, Ren S, Tao X, Liu J (2016) Enhanced plasticity by nanocrystallite in bulk amorphous $Al_2O_3-ZrO_2-Y_2O_3$. *Int J Plast* 79:314–327. doi:[10.1016/j.ijplas.2015.09.004](https://doi.org/10.1016/j.ijplas.2015.09.004)
- Zaiser M (2006) Scale invariance in plastic flow of crystalline solids. *Adv Phys* 55:185–245
- Zaiser M, Mill F, Konstantinidis A, Aifantis K (2013) Strain localization and strain propagation in collapsible solid foams. *Mater Sci Eng A* 567:38–45
- Zaiser M, Aifantis EC (2006) Randomness and slip avalanches in gradient plasticity. *Int J Plast* 22(8):1432–1455. doi:[10.1016/j.ijplas.2005.07.010](https://doi.org/10.1016/j.ijplas.2005.07.010) (special issue in honour of Dr. Kirk Valanis)
- Zaiser M, Moretti P (2005) Fluctuation phenomena in crystal plasticity—a continuum model. *J Stat Mech Theory Exp* 2015(08):P08004
- Zhou H, Zhong C, Cao Q, Qu S, Wang X, Yang W, Jiang J (2014) Non-localized deformation in metallic alloys with amorphous structure. *Acta Mater* 68:32–41